IEEE Access
Multidisciplinary ⋮ Rapid Review ⋮ Open Access Journal

Received January 23, 2020, accepted March 2, 2020, date of publication March 5, 2020, date of current version March 17, 2020.

Digital Object Identifier 10.1109/ACCESS.2020.2978524

Utilization of Oil Shale as an Electromagnetic Wave Absorbing Material in the Terahertz Range

HONGLEI ZHAN[1,2,5], MENGXI CHEN[2,3], YAN ZHANG[4], RU CHEN[5], KUN ZHAO[4,5], AND WENZHENG YUE[1]

[1]State Key Laboratory of Petroleum Resources and Prospecting, China University of Petroleum, Beijing 102249, China
[2]Beijing Key Laboratory of Optical Detection Technology for Oil and Gas, China University of Petroleum, Beijing 102249, China
[3]Key Laboratory of Oil and Gas Terahertz Spectroscopy and Photoelectric Detection, Petroleum, and Chemical Industry Federation, China University of Petroleum, Beijing 102249, China
[4]Quantum Exploration Materials and Technological Innovation Pioneering Laboratory, China University of Petroleum, Beijing 102249, China
[5]College of New Energy and Materials, China University of Petroleum, Beijing 102249, China

Corresponding author: Kun Zhao (zhk@cup.edu.cn)

This work was supported in part by the Science Foundation of China University of Petroleum, Beijing, under Grant 2462017YJRC029, Grant ZX20190163, and Grant 2462018BJC005, in part by the National Nature Science Foundation of China under Grant 11804392, and in part by the University-Industry Collaborative Education Program under Grant 201901066031.

ABSTRACT This study demonstrates that oil shale subjected to pyrolysis at 1000 °C strongly absorbs electromagnetic radiation in the terahertz (THz) range. Analyses reveal obvious differences between oil shale samples with and without pyrolysis, as well as between low-middle mature shale and oil shale samples. The electromagnetic absorption effect of oil shale subjected to pyrolysis conditions is demonstrated to be strongly related to its relatively small concentration of pyrite, which progressively yields pyrrhotite and elemental Fe during pyrolysis that facilitates the absorption of THz radiation. Accordingly, oil shale can be used not only as a resource for generating oil, natural gas, and petrochemical products, but the material obtained after processing can also be employed for the absorption of THz radiation as a means of converting incident electromagnetic radiation into heat or other forms of energy, which offers substantial prospects in many engineering and technology applications.

INDEX TERMS Oil shale, THz spectroscopy, wave absorbing, pyrite.

I. INTRODUCTION

Oil shale represents a tremendously prolific and predominantly untapped natural energy resource with many known deposits worldwide. Oil shale deposits are unconventional hydrocarbon sources that are of interest in a number of earth science disciplines, including petrophysics, geology, geophysics, and energy engineering [1]–[3], and are studied primarily because of their high kerogen content, which is of prime importance as a source of oil and natural gas [4]. Kerogen, which is a highly cross-linked and insoluble macromolecular solid material found in sedimentary rocks, represents the dominant source of organic compounds on the planet [5]. Typically, a single chemical formula is inadequate to represent kerogen, whose specific composition in oil shale depends on a long history of geological events and the thermal maturity of the shale. The kerogen in oil shale can be converted into oil, natural gas, and semi-coke by thermal degradation via pyrolysis under a temperature of 500 °C in an inert atmosphere [6].

The comprehensive utilization of oil shale for both chemical and energy extraction is a promising new technology that has achieved high utilization factors [7]. However, pyrite (FeS_2) is a common mineral found in oil shale deposits, and is also the main source of iron in oil shale residue and SO2 emissions formed when pyrite is oxidized. For example, oil shale collected from numerous regions in China has been found to contain pyrite in concentrations of approximately 5 wt% [8]. This is an important consideration in the comprehensive utilization of oil shale because the associated morphology of kerogen and pyrite has been shown to be an important factor affecting the pyrolysis of kerogen. Moreover, appropriate high-temperature conditions will reduce pyrite to iron ore, which may impart unexplored and potentially useful properties to oil shale. For example, a small amount of a metal may have a strong effect on the optical properties of oil

The associate editor coordinating the review of this manuscript and approving it for publication was Jenny Mahoney.

shale, making it useful as an optical material. Nonetheless, little research has been applied toward the development and utilization of pyrite in oil shale due to its relatively low content [9].

While few studies have explored the above-discussed alternative properties of oil shale, a considerable volume of research has considered these properties for the detection of oil shale, including some new technologies such as terahertz (THz) spectroscopy and laser [10]–[13]. Among these, THz spectroscopy in particular has been well exploited for characterizing both the structural and dynamical properties of materials [14], [15]. Moreover, the absorption of incident electromagnetic radiation in the THz region by appropriately absorbing materials can convert this electromagnetic radiation into heat or some other form energy. As such, materials that achieve a high degree of electromagnetic absorption in the THz range offer substantial prospects in many engineering and technology applications such as materials detection, biological sensing, microbolometers, and solar cells [16], [17]. Good THz absorbing materials are generally metallic composites, and were initially based on lossy dielectric magnetic slabs backed with metallic reflectors. At present, metamaterials are widely used as THz absorbers, and a variety of single-, dual-, multi-frequency, and broadband metamaterial absorbers have been proposed. However, these materials suffer from some shortcomings such as complex structures, high manufacturing requirements, and, in particular, high cost.

The present study addresses this issue by proposing the use of very inexpensive oil shale as a new THz absorbing material. Oil shale subjected to pyrolysis at 1000°C is demonstrated to absorb electromagnetic radiation strongly in the THz range. Analyses reveal obvious differences between oil shale samples with and without pyrolysis, as well as between low-middle mature shale and oil shale samples. The electromagnetic absorption effect of oil shale subjected to pyrolysis conditions is demonstrated to be strongly related to its relatively small concentration of pyrite, which progressively yields pyrrhotite and elemental Fe during pyrolysis that facilitates the absorption of THz radiation. Accordingly, oil shale can be used not only as a resource for generating oil, natural gas, and petrochemical products, but the material obtained after processing can also be employed for the absorption of THz radiation as a means of converting incident electromagnetic radiation into heat or other forms of energy.

II. EXPERIMENTAL

The oil shale deposits used in this research were collected from the Huadian district of Liaoning province, China. The mining depth of the oil shale materials was approximately 360 m. The oil shale material was cut into 2 mm thick slices, pyrolyzed at high temperatures, and allowed to cool in air for conducting THz absorption experiments. The surface morphologies of the oil shale samples and their entrained kerogen deposits were evaluated by scanning electron microscopy (SEM) to characterize the complex distribution and association of organic, mineral, and pore phases at the nano-to-micro scales [3]. In addition, the samples were further subjected to energy dispersive X-ray (EDX) spectroscopy analysis to evaluate the elemental compositions of the materials.

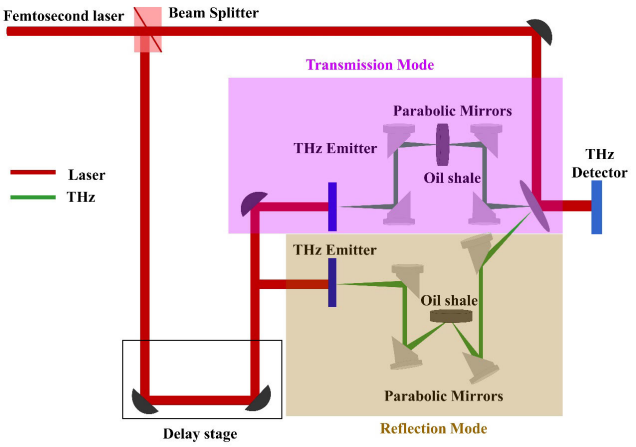

FIGURE 1. Schematic illustrating the THz time-domain spectroscopy (TDS) pump probe system with both transmission and reflection modes, and its use for evaluating the electromagnetic absorption properties of oil shale in the THz range.

A typical THz time-domain spectroscopy (TDS) system with both transmission and reflection modes was used for investigating the electromagnetic absorption properties of oil shale in the THz range. As shown in Fig. 1, the system consisted of an ultrafast laser, two THz emitters and a single detector, an optical delay line, a set of parabolic mirrors, and the oil shale samples. The optical beam pathways are shown in red and the THz beam pathways in green. The laser was diode-pump mode-locked with a center wavelength of 800 nm, a pulse width of 100 fs, and a repetition rate of 80 MHz. The laser beam was split into two beams with high and low optical power by a splitter, and the high power beam was used as the pump beam, while the low power beam was used as the probe beam. The THz emitters and detector were photoconductive antennae. The THz radiation emitted from the THz emitters was focused as collimated electromagnetic beams on the sample surfaces. Similarly, the THz radiation emitted from the sample surfaces was focused as collimated electromagnetic beams to meet the probe beam at the detector [18]. The THz signal was detected and amplified by a lock-in amplifier, which greatly increased the signal to noise ratio (SNR). A PC was used to control the measurement process and collect the signal data.

III. RESULT AND DISCUSSION

Figure 2 presents representative SEM images and the EDX results for the surface of an oil shale sample not subjected to pyrolysis. The SEM images exhibit highly variable surface morphologies, and mainly dispersed kerogen deposits can be clearly observed in Figs. 2(a)–(f) with a variety of shapes, such as strip-like and ball-like deposits. The EDX results

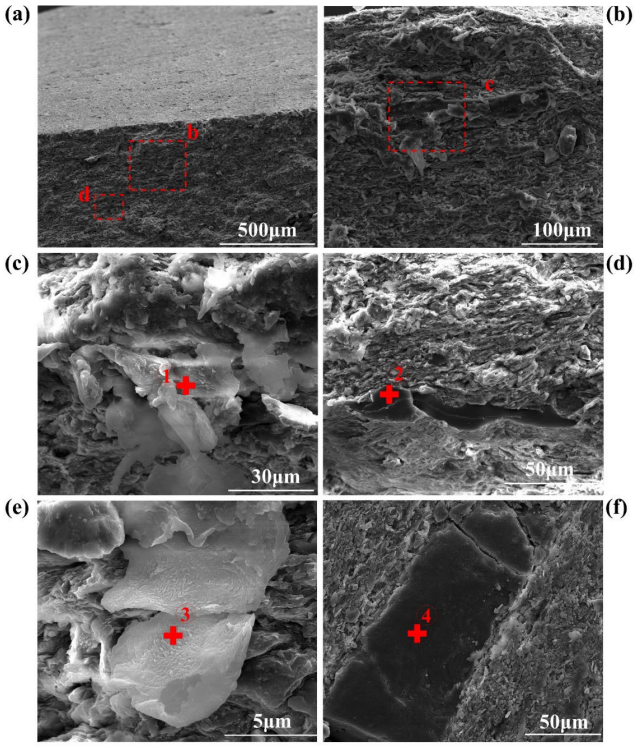

(g)

	C	O	Si	Al	Ca	Na	Cl
1	72.18	18.73	2.10	0	0	2.08	3.86
2	87.38	12.19	0	0	0.43	0	0
3	72.72	21.08	3.03	1.73	0	0	1.43
4	77.92	27.08	0	0	0	0	0

FIGURE 2. Direct scanning of kerogen in an oil shale sample without pyrolysis: (a) overview SEM image of the top surface and cross-section of an oil shale sample; (b) enlarged view of (a); (c) a further enlarged view of (b) exhibiting an obvious kerogen deposit; (d) enlarged view of (a) showing a kerogen deposit between mineral components; (e) another kerogen deposit similar to that shown in (c); (f) another kerogen deposit similar to that shown in (d); (g) EDX analysis results presenting the concentrations of various elements in the observed kerogen deposits shown in (c), (d), (e), and (f).

in Fig. 2(g) confirm that the darker areas are organic kerogen, and the lighter gray areas are an inorganic mineral matrix primarily composed of varying amounts of dolomite, calcite, quartz, and clays. The SEM and EDX analyses indicate that the kerogen in the oil shale sample is intimately associated and tightly bound with the heterogeneous mineral matrix. The mass fraction of carbon in the kerogen was observed to fall in the range 50–65 wt%.

As a preliminary investigation of the THz absorption of oil shale, Fig. 3 presents the THz field signal amplitude as a function of time after transmission or reflection of THz pulses through the air (as a reference) and oil shale samples without pyrolysis (25°C) and with pyrolysis at 1000°C. The heating rate was 10°C/min, and the furnace temperature was kept for 1 hour after reaching the target temperature. Comparison with the reference spectra obtained during transmission and reflection indicates that the THz signal peak intensities (EP) of the oil shale samples subject to pyrolysis at 1000°C

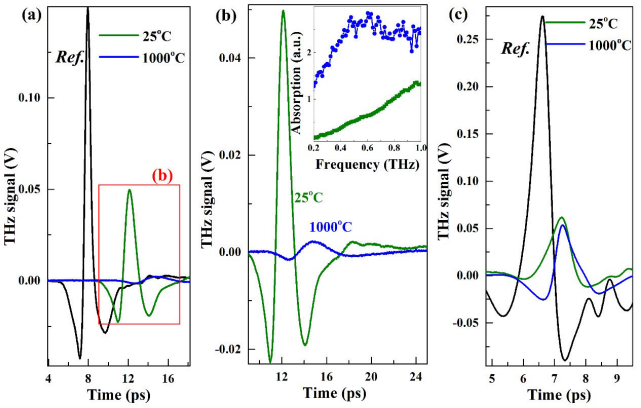

FIGURE 3. THz spectral analyses of oil shale samples without pyrolysis (25°C) and with pyrolysis at 1000°C: (a) transmission THz-TDS; (b) selected data in (a), where the inset presents the THz absorption of the oil shale samples in the 0.2–1.0 THz range; (c) reflection THz-TDS.

were attenuated to a much greater extent than the samples without pyrolysis under both conditions, which represents a strong absorption for the pyrolyzed samples in the THz range. Meanwhile, Fig. 3(a) and its enlarged view in Fig. 3(b) indicate that the characteristics of the THz transmission spectra obtained for the two samples differed substantially, showing that the physical properties can be differentiated using transmitted THz spectra. For example, the value of EP obtained for the oil shale sample at 25°C was 23 times greater than that of the sample pyrolyzed at 1000°C. In addition, the inset of Fig. 3(b) presents the frequency dependent absorbance spectra obtained according to the THz-TDS data in the 0.2–1.0 THz range. Here, we note that the oil shale sample pyrolyzed at 1000°C exhibited strong absorption over the entire range, particularly in the 0.5–1.0 THz range. Meanwhile, we note from Fig. 3(c) that the THz reflection spectra of the oil shale samples are quite similar in the THz range.

Oil shale samples pyrolyzed at 100°C were characterized by SEM in an effort to ascertain their THz absorption mechanism. Figures 4(a)–(h) present a number of SEM images, and the results of EDX analysis at points 1–8 are shown in Fig. 4(k). We note from Figs. 4(a) and (b) that numerous octahedral pyrite crystals were observed on the surface of the pyrolyzed sample, which is consistent with the high proportion of Fe and S shown in the EDX results for points 1 and 2. Moreover, the Fe/S ratio is approximately 1:2, which is consistent with the stoichiometric composition of FeS_2, indicating a high purity for the pyrite microcrystals. In addition, Figs. 4(c)–(h) indicate that pyrite microcrystals with a polyhedral structure were observed within kerogen deposits on the surface, which is consistent with the high proportion of C and O shown in the EDX results for points 3 and 5–8 with very little or no concentration of other elements associated with sandstone and carbonates (e.g., Si, Ca, and Mg). The individual pyrite microcrystals were approximately 0.1 to 3 μm in size. Moreover, the SEM images and corresponding EDX results indicate that the pyrite

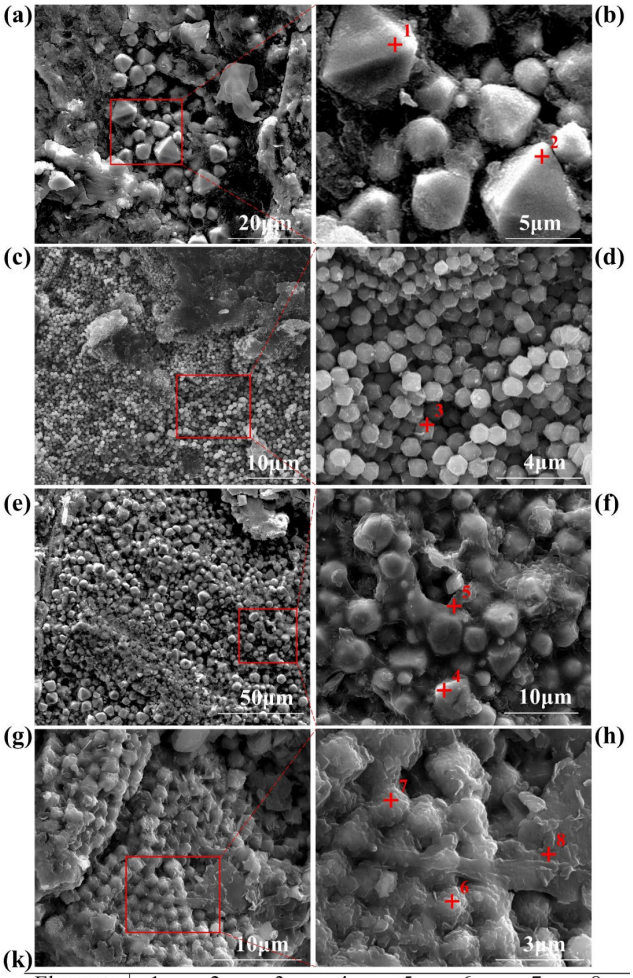

Element	1	2	3	4	5	6	7	8
C	0	0	59.92	0	64.09	22.37	21.82	22.77
O	0	0	13.46	0	10.61	16.63	20.80	33.30
S	66.34	65.57	16.16	64.07	15.66	39.86	37.73	19.38
Fe	33.66	34.43	8.54	33.99	9.63	21.14	19.65	9.31
Others	0	0	1.96	1.94	0	0	0	15.24

FIGURE 4. Microstructure and chemical analysis of minerals and inorganic mineral grains dispersed within kerogen deposits on an oil shale sample subjected to pyrolysis at 100°C: (a) overview SEM image of the oil shale sample surface showing large numbers of mineral particles; (b) enlarged view of (a) showing several octahedral pyrite crystals; (c) overview SEM image of uniformly sized mineral particles on the sample surface; (d) enlarged view of (c) showing numerous particles with diameters less than 1 μm; (e) overview SEM image of numerous pyrite crystals semi-wrapped in kerogen; (f) enlarged view of (e); (g) overview SEM image of uniformly sized pyrite particles coated with kerogen; (h) enlarged view of (g); (k) EDX analysis results showing the concentrations of various elements in the observed kerogen and pyrite deposits in (b), (d), (f), and (h).

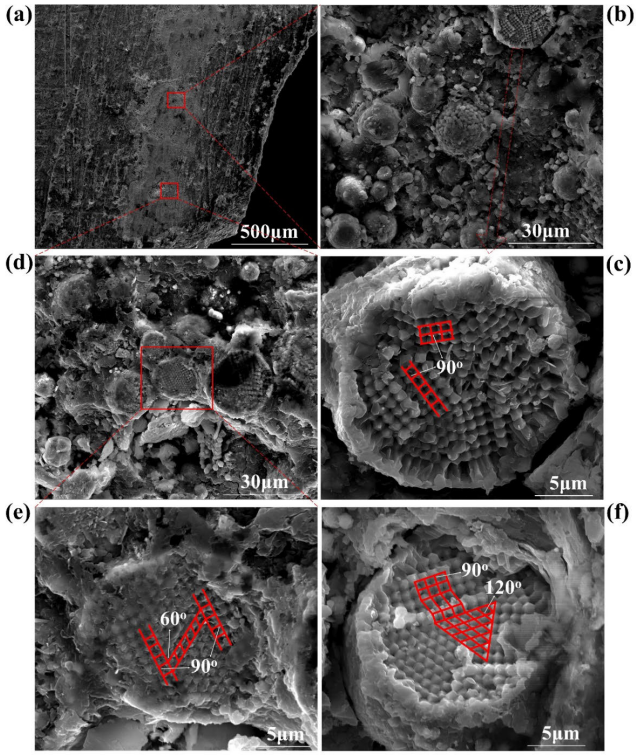

FIGURE 5. Analysis of spheroidal inclusions with diameters of ∼100 nm characteristic of kerogen deposits consisting of collections of evenly arranged polyhedron-shaped pyrites microcrystals on the surface of the pyrolyzed oil shale sample: (a) overview SEM image of the oil shale surface; (b) enlarged view of (a) showing several inclusions; (c) enlarged view of (b) showing a highly concentrated and regular right-angle arrangement of pyrite microcrystals; (d) another enlarged view of (a); (e) enlarged view of (d) showing a highly concentrated group of pyrite microcrystals with 60° or 90° arrangements; (f) another inclusion with a highly concentrated group of pyrite microcrystals with both 120° and 90° arrangements.

microcrystals were generally distributed unevenly and encapsulated within the kerogen deposits, but were at times packed closely together in a regular arrangement, as shown in the middle of the Fig. 4(g). Consequently, we can conclude that the kerogen was associated with the pyrite microcrystals.

As shown in Fig. 5, the oil shale sample pyrolyzed at 100°C also contained a significant number of spheroidal inclusions with diameters of ∼100 nm characteristic of kerogen deposits consisting of collections of evenly arranged polyhedron-shaped pyrite microcrystals, some of which are regular octahedrons with a smooth appearance and sharp edges, which are common in oil shale materials. As shown in Figs. 5(c), (e), and (f), some of the pyrite microcrystals were arranged at right angles, while some were arranged in an equilateral triangle at angles of 120°.

The results in Figs. 4 and 5 support the following conjectures regarding the associated formation of pyrite microcrystals and kerogen in Huadian oil shale. A high rate of subsidence during the deposition of the oil shale members caused significant deepening of the Huadian depositional lake, as well as high lacustrine productivity, and thereby providing abundant organic matter for oil shale formation. This inference is supported by biomarker data, which show that the organic matter preserved in the oil shale samples mostly consists of alginite (lamalginite and telalginite), with only small amounts of terrigenous organic matter. In this circumstance, sulfate-reducing bacteria were active owing to the sufficient supply of organic matter. Low productivity or high sedimentation rates caused dilution of the accumulated organic matter by detrital minerals (pyrite). The existence of kerogen and

pyrite together imparts the absorption characteristics of the oil shale in THz range.

The SEM and EDX results shown in Fig. 6 are evaluated here to explore the effect of morphology and composition of oil shale samples subjected to pyrolysis above 600°C in an effort to investigate the reason why THz absorption drastically increased when the oil shale sample was pyrolyzed at 1000 °C. As a baseline, we first considered the pyrite microcrystal cluster shown Figs. 6(a) and (b) for an oil shale sample subjected to pyrolysis at 100°C, which the EDX results indicate is composed of a fairly stoichiometric concentration of Fe and S indicative of FeS_2. From Fig. 6(c), we note that pyrite microspheres are obtained after pyrolysis at 650°C. The EDX results for points 2 and 3 in Fig. 6(d) indicate that the cluster mainly contained Fe and O with similar Fe/O ratios for both points, as well as a small amount of residual S. The existence of a small concentration of Si at point 3 is indicative of a silicate matrix. These results indicate that pyrite on the surface of the microspheres begins to decompose for a pyrolysis temperature greater than 500°C, and sulfur gas is released, resulting in the formation of an iron sulfide of lower sulfur content, i.e., pyrrhotite FeSx, where $1 \leq x < 2$, which was then subjected to successive oxidation. As such, the SEM image in Fig. 6(d) represents an incompletely oxidized pyrite particle with two different textures composed of a rim surrounding the particles that was retained from the direct oxidation of the pyrite at an earlier heating stage, and an inner part derived from the oxidation of the pyrrhotite. Interestingly, Fig. 6(e) shows that the pyrite microspheres subjected to pyrolysis at 700°C yield nanorods radiating outward from the broken pyrite microspheres. The EDX results for point 4 indicate that these nanorods are mainly composed of Fe and O, but S (18%) and a small concentration of other elements are also present. Clearly, these crystals consisted of iron oxides and incompletely oxidized pyrrhotite. As shown in Figs. 6(f) and (g), the most striking feature of the crystal clusters in the oil shale samples pyrolyzed at 750°C and 800°C was that the concentration of Fe was much greater than that of the other elements, particularly at 800°C, where the Fe concentration was as high as 95%, indicating that FeS_2 is reduced to elemental Fe in the process [19], [20]. Meanwhile, we plotted the THz-TDS of oil shale samples pyrolyzed at 100, 650, 750, 800°C in Fig. 7, showing that THz absorption of oil shale became very strong when the pyrolysis temperature was larger than 750°C.These results indicate that pyrite proceeded through a multi-step process with increasing pyrolysis temperature according to the following sequence: pyrite (FeS_2) → pyrrhotite [(FeS)N(S2)1−N, $0.91 \leq N \leq 1$] → Fe. It is well known that metal has a small transmittance in the THz frequency range. As such, these results may help to explain why the THz absorption drastically increased when the oil shale sample was pyrolyzed at 1000°C.

We note that low-middle mature shale is composed of layered structures that are similar to those of oil shale. Therefore, we also evaluated the THz transmission spectra, surface morphologies, and chemical compositions of

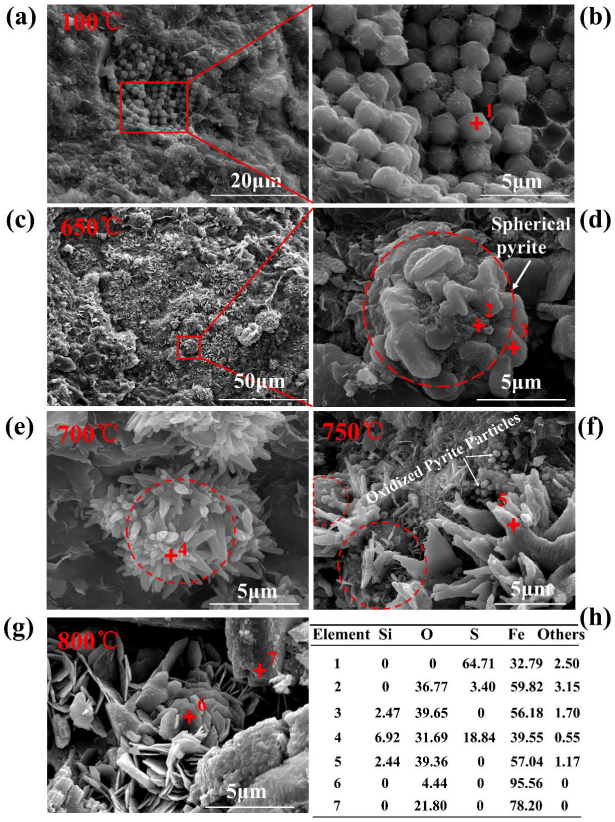

Element	Si	O	S	Fe	Others
1	0	0	64.71	32.79	2.50
2	0	36.77	3.40	59.82	3.15
3	2.47	39.65	0	56.18	1.70
4	6.92	31.69	18.84	39.55	0.55
5	2.44	39.36	0	57.04	1.17
6	0	4.44	0	95.56	0
7	0	21.80	0	78.20	0

FIGURE 6. Morphology and elemental analysis of pyrite inclusions within oil shale samples pyrolyzed at various temperatures: (a) SEM image of oil shale pyrolyzed at 100°C showing a number of pyrite particles; (b) enlarged view of pyrite particles in (a); (c)–(g) SEM images of pyrite products in oil shale pyrolyzed to semi-coke at 650°C, 700°C, 750°C, and 800°C, respectively; (h) EDX analysis results at different locations of the oil shale samples.

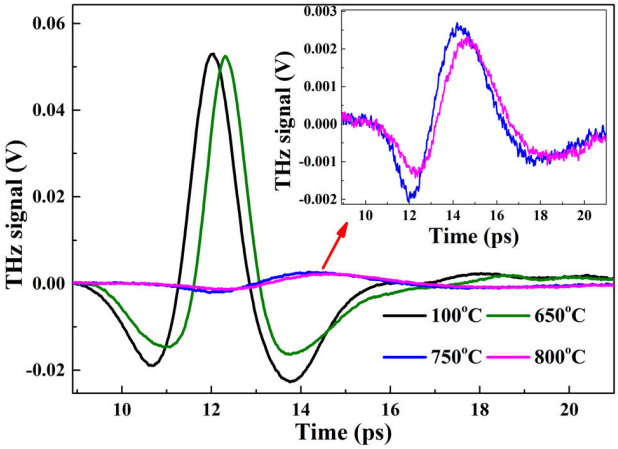

FIGURE 7. THz-TDS of oil shale samples pyrolyzed at 100, 650, 750, 800°C, Which corresponded to Figure 6.

low-middle mature shale samples without pyrolysis (25°C) and with pyrolysis at 1000°C for comparison with the oil shale samples. As shown in Fig. 8(a), the waveforms of the THz transmission spectra differ substantially from those of the corresponding oil shale samples given in Fig. 3(a) in

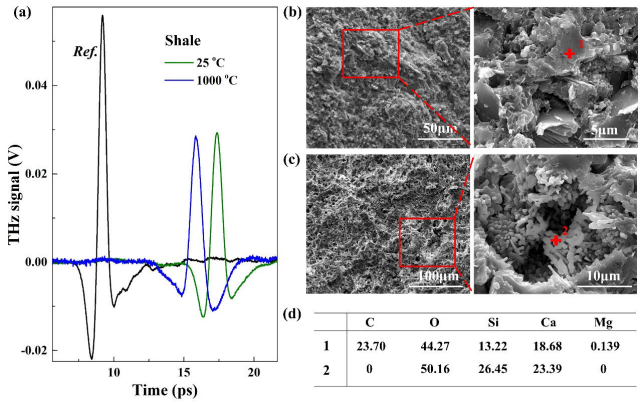

FIGURE 8. THz spectral analysis, SEM images, and EDX analyses of low-middle mature shale samples without pyrolysis (25°C) and with pyrolysis at 1000°C: (a) transmission THz-TDS; (b) SEM image of the original shale sample; (c) SEM image of pyrolyzed shale sample; (d) EDX analyses of shale samples in (b) and (c) with principal components consisting of carbonates/silicates and nanometer rod oxides, respectively.

terms of the EP values and the peak time positions, which indicates that shale and oil shale samples can be differentiated based on THz transmission spectra. The EP values of the shale samples with and without pyrolysis were equal, and both signals were attenuated by approximately half compared to the reference. This indicates that shale is not a strong wave absorber in the THz range with or without pyrolysis. The SEM images shown in Figs. 8(b) and (c) reveal similar morphologies and anisotropic features to those of oil shale, particularly when subjected to pyrolysis at 1000°C, where numerous nanometer rods are observed. However, the EDX results shown in Fig. 8(d) indicate that the principal components of the shale sample without pyrolysis were carbonates and silicates, while the principal components of the shale sample subjected to pyrolysis were oxides. Therefore, while oil shale and shale had similar morphologies and anisotropic features, they contained different organic materials and minerals. The absence of pyrite in the shale is a distinctive feature indicative of the role of pyrite in the strong THz absorption of the pyrolyzed oil shale samples.

IV. CONCLUSION

In summary, oil shale was verified to be an effective electromagnetic absorbing material in the THz range. Analyses based on THz-TDS, SEM images, and EDX results revealed obvious differences between oil shale samples with and without pyrolysis, as well as between low-middle mature shale and oil shale samples. Oil shale reflected small absorption effect and reflectivity, while the pyrolyzed oil shale at high temperature exhibited low transmittance and reflectivity, simultaneously. This proved oil shale to be a natural THz wave absorbing material, indicating that oil shale can be widely used as optical material after pyrolyzed for oil and gas resources. The pyrite in oil shale was the key component for the wave absorbing effect. When decomposed into pyrrhotite and element Fe, oil shale converted the incident electromagnetic wave into other energy. This research reported a new application of oil shale as THz wave absorber and revealed the mechanism of wave absorbing, which would promote economic benefit of oil shale.

REFERENCES

[1] M. Dai, Z. Yu, S. Fang, and X. Ma, "Behaviors, product characteristics and kinetics of catalytic co-pyrolysis spirulina and oil shale," *Energy Convers. Manage.*, vol. 192, pp. 1–10, Jul. 2019.
[2] Y. Huang, M. Zhang, B. Deng, H. Kong, Y. Zhang, J. Lyu, H. Yang, and Y. Jin, "Two-dimensional combustion modelling and experimental research on oil shale semicoke," *Fuel*, vol. 256, Nov. 2019, Art. no. 115891.
[3] T. Saif, Q. Lin, A. R. Butcher, B. Bijeljic, and M. J. Blunt, "Multi-scale multi-dimensional microstructure imaging of oil shale pyrolysis using X-ray micro-tomography, automated ultra-high resolution SEM, MAPS mineralogy and FIB-SEM," *Appl. Energy*, vol. 202, pp. 628–647, Sep. 2017.
[4] Q. Wang, Y. Hou, W. Wu, M. Niu, S. Ren, and Z. Liu, "The relationship between the humic degree of oil shale kerogens and their structural characteristics," *Fuel*, vol. 209, pp. 35–42, Dec. 2017.
[5] X. X. Han, X. M. Jiang, and Z. G. Cui, "Studies of the effect of retorting factors on the yield of shale oil for a new comprehensive utilization technology of oil shale," *Appl. Energy*, vol. 86, no. 11, pp. 2381–2385, Nov. 2009.
[6] M. Niu, S. Wang, X. Han, and X. Jiang, "Yield and characteristics of shale oil from the retorting of oil shale and fine oil-shale ash mixtures," *Appl. Energy*, vol. 111, pp. 234–239, Nov. 2013.
[7] Y. Lin, Y. Liao, Z. Yu, S. Fang, Y. Lin, Y. Fan, X. Peng, and X. Ma, "Co-pyrolysis kinetics of sewage sludge and oil shale thermal decomposition using TGA–FTIR analysis," *Energy Convers. Manage.*, vol. 118, pp. 345–352, Jun. 2016.
[8] M. Pathak, H. Kweon, M. Deo, and H. Huang, "Kerogen swelling and confinement: Its implication on fluid thermodynamic properties in shales," *Sci. Rep.*, vol. 7, no. 1, Oct. 2017, Art. no. 12530.
[9] K. Siedenberg, H. Strauss, O. Podlaha, and S. van den Boorn, "Multiple sulfur isotopes (δ^{34}S, Δ^{33}S) of organic sulfur and pyrite from Late Cretaceous to Early Eocene oil shales in Jordan," *Organic Geochemistry*, vol. 125, pp. 29–40, Nov. 2018.
[10] H. Zhan, M. Chen, K. Zhao, Y. Li, X. Miao, H. Ye, Y. Ma, S. Hao, H. Li, and W. Yue, "The mechanism of the terahertz spectroscopy for oil shale detection," *Energy*, vol. 161, pp. 46–51, Oct. 2018.
[11] H. Zhan, K. Zhao, and L. Xiao, "Spectral characterization of the key parameters and elements in coal using terahertz spectroscopy," *Energy*, vol. 93, pp. 1140–1145, Dec. 2015.
[12] H. Zhan, S. Wu, R. Bao, L. Ge, and K. Zhao, "Qualitative identification of crude oils from different oil fields using terahertz time-domain spectroscopy," *Fuel*, vol. 143, pp. 189–193, Mar. 2015.
[13] Y. Z. Li, S. X. Wu, X. L. Yu, R. M. Bao, Z. K. Wu, W. Wang, H. L. Zhan, K. Zhao, Y. Ma, J. X. Wu, S. H. Liu, and S. Y. Li, "Optimization of pyrolysis efficiency based on optical property of semicoke in terahertz region," *Energy*, vol. 126, pp. 202–207, May 2017.
[14] H. Zhan, Q. Li, K. Zhao, L. Zhang, Z. Zhang, C. Zhang, and L. Xiao, "Evaluating PM2.5 at a construction site using terahertz radiation," *IEEE Trans. Terahertz Sci. Technol.*, vol. 5, no. 6, pp. 1028–1034, Nov. 2015.
[15] E. Castro-Camus, M. Palomar, and A. A. Covarrubias, "Leaf water dynamics of arabidopsis thaliana monitored *in-vivo* using terahertz time-domain spectroscopy," *Sci. Rep.*, vol. 3, no. 1, Oct. 2013, Art. no. 1038.
[16] R. M. Bao, F. K. Qin, R. Chen, S. T. Chen, H. L. Zhan, K. Zhao, W. Z. Yue, "Optical detection of oil bearing in reservoir rock: Terahertz spectroscopy investigation," *IEEE Access* vol. 7, pp. 121755–121759, 2019.
[17] Y. T. Zhao, B. Wu, B. J. Huang, and Q. Cheng, "Switchable broadband terahertz absorber/reflector enabled by hybrid graphene-gold metasurface," *Opt. Express*, vol. 25, no. 7, pp. 7161–7169, Mar. 2017.
[18] H. Zhan, S. Sun, K. Zhao, W. Leng, R. Bao, L. Xiao, and Z. Zhang, "Less than 6 GHz resolution THz spectroscopy of water vapor," *Sci. China Technol. Sci.*, vol. 58, no. 12, pp. 2104–2109, Oct. 2015.
[19] H. Qin, Z. Hao, Q. Wang, and J. Bai, "Sulfur release from oil shale in retort," *Energy Procedia*, vol. 17, pp. 1747–1753, 2012.
[20] G. Hu, K. Dam-Johansen, S. Wedel, and J. P. Hansen, "Decomposition and oxidation of pyrite," *Progr. Energy Combustion Sci.*, vol. 32, no. 3, pp. 295–314, Jan. 2006.

HONGLEI ZHAN was born in 1991. He received the B.Sc. degree from Xiamen University, Xiamen, China, in 2012, and the Ph.D. degree from the China University of Petroleum, Beijing, China, in 2017. He is currently the Head of the Key Laboratory of Oil and Gas Terahertz Spectroscopy and Photoelectric Detection, Petroleum, and Chemical Industry Federation. His research interests focus on nano-petrophysics and the application of terahertz waves.

MENGXI CHEN was born in 1995. She received the bachelor's degree in polymer material and engineering from the Beijing University of Chemical Technology, Beijing, China, in 2017. She is currently pursuing the Ph.D. degree in material science and engineering with the China University of Petroleum, Beijing. Her research interests focus on the application of terahertz waves.

YAN ZHANG was born in 1995. She received the bachelor's degree from Liaocheng University, Shandong, China, in 2018. She is currently pursuing the master's degree in materials science and engineering with the China University of Petroleum, Beijing, China. Her research interest focuses on functional design studies of shale materials.

RU CHEN was born in 1994. He received the B.Sc. degree from Qufu Normal University, Jining, China, in 2017. He is currently pursuing the Ph.D. degree in material science and engineering with the China University of Petroleum, Beijing, China. His research interests focus on the application of terahertz waves and oblique-incidence reflection.

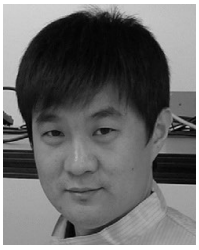

KUN ZHAO was born in 1971. He received the B.Sc. degree in physics from Nanjing University, Nanjing, China, in 1992, the master's degree from the Institute of Physics, Chinese Academy of Sciences, Beijing, China, in 1997, and the Ph.D. degree from The Chinese University of Hong Kong, Hong Kong, in 2001. He is currently a Professor in material science and engineering. His research interest is in oil and gas optics.

WENZHENG YUE received the Ph.D. degree from the China University of petroleum, Beijing. He is currently a Professor with the China University of petroleum. He has published over 60 articles in journals and international refereed conferences. His research interests are in well logging and rock physics.